Title
Electrostatic Side-Drive Rotary Stage on Liquid-Ring Bearing

Journal
Journal of Microelectromechanical Systems, 23(1)

ISSN
1057-7157

Authors
Sun, Guangyi
Liu, Tingyi
Sen, Prosenjit
et al.

Publication Date
2014-02-01

DOI
10.1109/jmems.2013.2262592

Peer reviewed

Authors' final manuscript for: G. Sun, T. Liu, P. Sen, W. Shen, C. Gudeman and C.-J. Kim, "Electrostatic Side-Drive Rotary Stage on Liquid-Ring Bearing," *J. Microelectromechanical Systems*, Vol. 23, 2014, pp. 147-156. (doi: 10.1109/JMEMS.2013.2262592)

Electrostatic Side-Drive Rotary Stage on Liquid-Ring Bearing

Guangyi Sun, Tingyi "Leo" Liu, Prosenjit Sen, Wenjiang Shen, Chris Gudeman, and Chang-Jin "CJ" Kim

***Abstract*— We present an electrostatically actuated rotary stage featuring liquid rings, which serve as both mechanical bearings and electric connections between the rotor and the substrate. The liquid rings are formed by confining a liquid inside hydrophilic grooves and repelling it from the superhydrophobic surfaces outside the grooves. Made of a fluid, the liquid-ring bearing avoids the dry friction of the solid bearings, significantly improving the reliability. Formed as rings, it avoids the resistance of contact-angle hysteresis sliding over droplets, and hence dramatically reducing the static friction. Furthermore, surface tension facilitates the self-alignment of the rotor to the substrate and stator during the assembly and provides the stability against drift and shock during operation. Electrically, each liquid ring passes an independent electric signal, allowing a direct electrical path between the substrate and potential components on the rotor. A three-phase electrostatic rotary stage has been design, fabricated, and tested. The minimum torque to initiate the rotation is ~2.5nN·m – hundreds of times smaller than droplet-based counterparts. The device has operated successfully by applying sequential voltages of $50V_{DC}$ between the rotor and the stators. The electric transmission has been verified by powering an LED on a rotating rotor. This is the first report of an electrostatically actuated rotating microdevice with a liquid bearing and a direct power transmission.**

***Index Terms*— Liquid bearing, liquid ring bearing, rotary stage, electrostatic actuation, ionic liquid, superhydrophobic, through-silicon-vias (TSVs)**

This work is supported by the Defense Advanced Research Projects Agency (DARPA) under grant W31P4Q-10-1-0008.

G. Sun, T. Liu and C.-J. Kim are with the Mechanical and Aerospace Engineering Department, University of California at Los Angeles, Los Angeles, CA 90095, USA. (e-mail: guangyi@ucla.edu; leolty@ucla.edu; cjkim@ucla.edu)

P. Sen was with the Innovative Micro Technology (IMT), Santa Barbara, CA 93117, USA. He is now with Centre for Nano Science and Engineering Indian Institute of Science, Bangalore, India. (e-mail: prosenjits@gmail.com)

W.Shen was with the Innovative Micro Technology (IMT), Santa Barbara, CA 93117, USA. He is now with Suzhou Institute of Nano-tech and Nano-Bionics, Chinese Academy of Sciences. (e-mail: wjshen2011@sinano.ac.cn)

C. Gudeman is with the Innovative Micro Technology (IMT), Santa Barbara, CA 93117, USA. (email: Chris@imtmems.com)

I. INTRODUCTION

A miniature rotating stage, on which other devices can be mounted and operated electrically by an external user, is an enabling platform for new applications in many areas including biomedical, electronic, and optical. For example, a robust rotary stage may add the capability of mechanical motions (positioning, inertial effect, etc.) to lab-on-a-chip devices for additional sample handling functions, to micro inertial sensors for in-field calibration, and to micro mirrors for azimuth control. A variety of miniature rotating devices have been reported over two decades featuring different types of bearings and actuation methods. Micromotors with solid bearings, including surface dimples [1], [2] and micro balls [3] [4], have been actuated electrostatically [1], [2]. [3] [4], ultrasonically [5], magnetically [6], etc. However, the solid-solid friction, which manifests its effect more strongly in microscale, calls for a high voltage, large current, or external magnet, etc. to actuate the device and may even lead to a visible wear [7]. Gas bearings [8], [9], [10], created through pneumatic [8], [9], [10], electrostatic [11], or magnetic [12] levitation avoid the surface friction altogether. However, the levitation requires complicated dynamic control mechanism and fabrication processes. Also the devices tend to suffer from a limited range of a stable operation.

As the third option, liquid bearings are expected to avoid the solid-solid friction as well as the complexity of levitation that the gas bearings require. Recently, liquid bearings in the form of a single rotor-sized droplet [13], [14] have been reported. Takei, Matsumoto, and Shimoyama [13] reported a rotating capillary motor composed of a floating plate (rotor) on a large droplet. Although we consider the droplet as a bearing for our categorization, the droplet is actually an electrowetting-based actuator. A relationship between the rotation (step response), the rotor (floating plate) geometries, and the liquid volume was experimentally observed. However, the rotor was found vibrating at low speeds (e.g., 120 rpm), and the uncertainty of its positioning (±2°) was large due to defects or nonuniformity in the hydrophobic layer. Chan et al. [14] reported a magnetically driven micro motor using a large droplet as the bearing. Because the rotor was found tilting, subsequently Yoxall et al. [15] added satellites droplets to prevent the rotor-substrate contact, which increased the minimum startup torque to 0.3 μN·m. While the rotor assembly was micromachined in both the cases [14], [15], unfortunately the magnetic actuation required permanent magnets on the rotor and a conventional electromagnetic coil placed below the assembly. In addition to

the above friction issue, perhaps more importantly for the utility of such devices, none of the reported micro rotating devices could transmit appreciable electrical power to the top of the rotor.

By fully utilizing the surface tension in the micromechanical design, in this paper we introduce multiple concentric rings of a conductive liquid as both mechanical bearings and direct electric connections between the rotor and the substrate. In addition to the obvious advantages of liquid bearings taken by the above liquid-bearing micro motors [13], [14] over the solid and gas bearings, a liquid bearing in the form of rings solves several important problems in a elegantly simple way. Compared with a single liquid droplet [13], multiple liquid rings (assuming conductive) provide multiple paths of direct electric connection – necessary to operate the independent devices on the rotor. Compared with multiple droplets [15], concentric rings rotate with no advancing or receding meniscus, i.e., no contact-angle hysteresis and essentially no static friction. Table I provides a brief comparison between the liquid-ring bearing of this paper and other reported micro bearing technologies.

By studying the mechanics, payload capability, electric conductivity, and electrochemical properties of rings made of an ionic liquid, we have recently designed a miniature rotary stage featuring ionic liquid rings as both mechanical bearings and electric connections between the rotor and the substrate [16], for the first time. In order to reduce the design into practice, we have developed several fabrication techniques, including formation and patterning of black-silicon superhydrophobic surfaces and formation of through-silicon-via (TSV) in silicon-on-insulator (SOI) wafers. The rotary stage was driven by a three-phase electrostatic actuation from the side stators outside the rotor. Separately, a direct transmission of electrical power was verified by powering an LED on a rotating rotor (> 300 rpm) from the substrate. While the electrostatic actuation and power transmission were implemented and demonstrated separately in preliminary results [16], here we report an integrated device featuring both electrostatic actuation and power transmission simultaneously. Besides, we also report additional studies, technical details, and quantified characterization, including: principles of liquid-ring bearings, design of the electrostatically side-driven rotary stage, fabrication, assembly, and characterization of the device, and further discussion of the results.

II. PRINCIPLES AND DESIGN

The rotary stage presented in this paper is composed of four main components: rotor, liquid-ring bearing, stators, and substrate, as shown in the exploded view of Fig. 1. Figure 2 shows an assembled device with a cut-off view to reveal the two liquid rings and several TSVs. The liquid rings not only support the rotor and lubricate its rotation as a mechanical bearing but also make the rotor electrically connected with the substrate. The stage is operated by rotating the rotor using the electrostatic forces between the rotor and the stators, while electric signals are transmitted between the substrate and the top of the rotor through the liquid rings and TSVs. An ionic liquid has been chosen to form the liquid rings for its properties of good electric conductivity, very low vapor pressure (virtually no evaporation), good thermal stability and high surface tension comparable to water. Direct electric transmission to and from a fully rotating component of a micro device has never been reported, to the best of our knowledge.

A. Liquid Ring as Mechanical Bearing

As shown in Figs. 1 and 2, a rotor and a substrate each has two circular grooves, along each of which a liquid ring is formed. For a direct transmission of electrical signals, at least two separate liquid rings are required. The two grooves are concentric (Φ_{inner} = 1 cm; Φ_{outter} = 2 cm) and have the same width (W = 1 mm) and depth (D = 100 μm). The inner surfaces of the grooves are highly wetting (apparent contact angle ~ 0° after oxygen -plasma treatment) while the outside surfaces are highly non-wetting (apparent contact angle > 150°) to the ionic liquid used. This highly contrasted wetting condition confines the liquid inside the grooves and repels it from the outer surfaces. Note that, unlike sliding a liquid droplet along a circular path [15], sliding a liquid ring along its circular path does not incur any meniscus deformation so that no static resistance resulted from the contact angle hysteresis, at least in theory.

Figure 2a shows how the liquid ring acts as a mechanical bearing. Because the rotor-substrate gap h_l (i.e. liquid ring height) is much smaller than the size of the rotor and the ring geometries, we can reasonably approximate

that the Laplace pressure within each liquid ring and the meniscus angle along the liquid rings are identical. In vertical direction, the weight of the rotor (including payload) is balanced by Laplace pressure and surface tension of the liquid rings:

$$W = F_{\Delta p} - F_{\gamma} = \Delta P \cdot A_{rings} - \gamma \sin\alpha \cdot C_{rings} \quad (1)$$

where W is the rotor weight, $F_{\Delta P}$ is the supporting force from Laplace pressure ΔP, F_{γ} is the pull-down force by liquid surface tension γ, α is the meniscus angle the liquid makes with the outer surface at the edge of the grooves, A_{rings} is the total projected area of the grooves' bottom surfaces, and C_{rings} is the total circumferential length of the grooves. If the rotor-substrate gap h_l decreases by an additional weight (i.e. static load) or an upward acceleration (i.e. dynamic load), the Laplace pressure ΔP and thus the supporting force $F_{\Delta P}$ increase, resisting further decrease of the gap h_l, until the meniscus angle α exceeds the advancing contact angle of the liquid on the highly non-wetting outer surfaces (>150°). Therefore, the rotor weight and its payload weight are determined by the minimum gap.

On the other hand, if the rotor-substrate gap h_l increases excessively (e.g. by a downward acceleration), a negative Laplace pressure ΔP together with the liquid surface tension γ pulls the rotor downward, again keeping the rotor within a vertical range. As a matter of fact, this pulling action assists one to assemble the rotor to the substrate during the device fabrication. Besides, even if the device is flipped over the rotor can withstand gravity due to this pulling action before the gap h_l reaches its maximum value.

Figure 2b illustrates the self-centering nature of the liquid rings. If the rotor is shifted off its aligned position with the substrate, stretching the menisci of the liquid ring, the surface tension pulls the rotor back toward the aligned position to restore the minimum energy state. One can increase the restoring forces by increasing the number of liquid rings in the device design. In addition to the vertical and horizontal stabilities, well-designed liquid rings also provide a restoring force against the tilting of the rotor, as proven later experimentally [17]. Overall, the rotor becomes more robust – more resistant to collapsing, shifting, and tilting – as the gap h_l is reduced. For the device presented in this paper, the rotor-substrate gap h_l is maintained in a range of 100 – 200 μm, which is much smaller than the ring width (W = 1 mm) and ring diameters (R_{inner} = 5 mm; R_{outer} = 10 mm), in order to have a good

stability. The current height of 100-200 μm was found most feasible and repeatable with respect to liquid volume control and assembly of rotor, based on the experience from fabrication development. Smaller liquid height requires more accurate liquid volume control.

B. Electric Power and Signal Transmission

Electric current *i* flows between the substrate and the top of the rotor through the liquid rings and the TSVs, as indicated in Fig. 2c. The rotor is made from an SOI wafer highly doped to be conductive for electrostatic actuation. Because each liquid ring is to serve as an independent electrical path, an isolation trench is made into the handle side of the SOI wafer to ensure a good electrical isolation between two liquid rings for low frequency signals. See the top figure of Fig. 2 to identify the isolation trench.

We have considered two different types of materials for the liquid ring: liquid metals and ionic liquids. Liquid metals, e.g., mercury or Galinstan®, have a very high surface tension and excellent electric conductivity, both of which are highly attractive properties to our liquid ring bearings. However, most liquid metals oxidize on the surface and require a special operation environment or advanced packaging to prevent formation of an oxide shell [18], which makes the use of liquid metals difficult. Alternatively, we chose to use an ionic liquid for the liquid-ring bearing.

Unlike metals or semiconductors, the charge carriers for ionic liquids are ions. While ionic liquids are frequently studied and utilized for their physical and chemical properties and as an electrolyte [19], [20], [21], [22], few utilize ionic liquid as an electric component for micro devices [23], [24]. In order to deliver an appreciable electrical power for our applications, an ionic liquid with a relatively large electrochemical window and high electrical conductivity is preferred. The electrochemical window is the voltage range in which the ionic liquid functions as desired, i.e., without getting oxidized or reduced. After reviewing the Ionic Liquids Database (ILThermo) from the National Institute of Standards and Technology (NIST) [25], we chose 1-Ethyl-3-methylimidazolium dicyanamide (EMIM DCA, $C_8H_{11}N_5$) (Sigma-Aldrich®) for its relatively high

conductivity (27 mS/cm), low dynamic viscosity (15-20 mPa•s), and high surface tension (64 mN/m) [22]. In addition to the electric current in the ionic liquid, the current between the metal electrode and the ionic liquid must be taken into consideration because of the potential electrochemical reaction at the metal-liquid interface. Since gold has been confirmed as not reactive with EMIM DCA within the electric current range for power transmission studied in this report, the bottom of the grooves was covered with gold, as shown in Fig. 2. In order to avoid electrolysis, however, the voltage applied across the ionic liquid should not exceed its electrochemical window.

C. Electrostatic Actuation

Compared with other mechanisms, electrostatic actuation is the most compatible with the planar processes of integrated circuit (IC) fabrication. This leads to a batch fabrication and low-cost product and consumes the least power for operation, which is attractive to off-the-grid applications such as distributed sensors. Since the direct (i.e., gap-closing) electrostatic attraction is not stable by nature, most micro devices use the fringe-field attraction, which unfortunately is much weaker and requires a mechanical provision (e.g., flexure beams [26], [27]) to prevent the gap closing. The liquid-ring bearing addresses the above two main limitations with its unique properties: very small static friction against rotation and inherent stability against physical disturbances.

The rotary stage in this work uses a three-phase, side-driven electrostatic actuation, which has been widely reported for micro devices. The stators are made of highly doped silicon and coated with Au on top. In order to increase the electrostatic torque, both the rotor and stators contain multiple teeth-like electrodes, as each tooth contributes two fringe fields. The step size Θ of the rotation can be estimated by the total number of teeth on the rotor n_r and that on the stators n_s:

$$\Theta = 360^{o} \cdot \left(\frac{1}{n_r} - \frac{1}{n_s + 12}\right) \cdot \left(\frac{n_s}{6} + 2\right) \tag{2}$$

Here, $n_r = 56$ and $n_s = 42$, which results in $\Theta \approx 2°$. The empty spaces between the adjacent stators (Fig. 2) make two teeth missing per stator; if not, n_s could have been 54. Both the rotor and the substrate are made of a ~350

μm-thick SOI wafer, and the stators are of ~500 μm-thick silicon wafer, so that the rotor is always within the stator thickness over a range of rotor-substrate gap (h). What is more critical is the gap between the rotor and the stators, since the rotor tends to snap to the surrounding stator electrodes at high voltage actuations if the rotor-stator gap (g) is not uniform. Considering the capability of the UCLA cleanroom and the practical limitations of manual assembly, we designed the device in this work with g = 100 μm.

A three-phase voltage was applied sequentially between the three pairs of diagonally opposite stators while the rotor in the middle was electrically floating all the time. The voltage between an activated stator and the rotor generated an electrostatic force. The tangential (fringe-field) component of the electrostatic force generated a torque, which pulls the teeth of the rotor to realign with those of the activated pair of stators. The torque T is determined by the applied voltage V and the angular position of the rotor θ,

$$T(V,\theta) = \frac{1}{2} V^2 \frac{\partial C(\theta)}{\partial \theta} \tag{3}$$

where $C(\theta)$ is the capacitance between the activated stator and the rotor [1]. For a given geometry design, the torque T can be analytically evaluated or simulated using finite-element method (FEM). When the teeth of the activated stators are maximally aligned with those of the rotor, the teeth of the other two pairs of stators have a maximum misalignment. Subsequently, the driving voltage is switched to another phase, activating the next pair of stators. Based on the above analysis, the rotary stage has been fabricated with the geometric specifications listed in Table II.

D. Finite Element Analysis

We used finite element analysis (FEA) to estimate the torque generated by the electrostatic force. Following the geometric specifications in Table II, two-dimensional (2D) models of rotor and surrounding stators were built and simulated by Comsol 3.5. Due to the limitations of memory and computational capability, 2D models were used instead of full 3D models by simply giving thickness information for the 2D models. Figure 3a shows the overall 2D model of the rotary stage and an exemplary simulation result of the electrostatic field between the rotor and the stator. In the FEA simulation, the rotor was set to be ground while the outer stator was set to be of an input

voltage of 50 $V_{DC.}$ Due to the electrostatic force between the rotor and the stator, the rotor is about to rotate counter-clockwise from the initial point ($\theta = 0$). In order to investigate the relationship between the output torque T and the angular position of the rotor θ, we simulated the trend of output torque for two continuous phases: phase I and phase II (stators I and II) as shown in Fig. 3b. When the rotor and the active stator completely match, the actual torque goes to zero and the next stator is subsequently activated. Although the maximum torque was estimated to be ~3.2 nN.m, the start-up torque at the switching point was ~2.5 nN.m, i.e., ~78% of the maximum. Furthermore, it is obviously not an optimized switching point to activate the next stator till the torque goes down to zero. In fact, from Fig. 3b, we can see that in the transmission zone the electrostatic force in the two phases are in the same direction, which means if both two stators are activated the output torque remains at the start-up value without further decrease. Lacking a feedback position sensing, however, the current device cannot obtain the optimized switching point, which limits the rotational speed.

III. FABRICATION AND ASSEMBLY

A. Fabrication of Rotor and Substrate

The rotor and the substrate are fabricated from a highly doped SOI wafer (150 mm diameter; 250 μm handle layer; 1 μm buried oxide, ~ 500 μm device layer) by a deep reactive ion etching (DRIE), TSV process, and formation of a superhydrophobic surface, as well as the conventional IC fabrication steps, as illustrated in Figure 4. First, multiple TSVs (60 μm in diameter; 250 μm deep) were formed in the handle layer by making via holes by DRIE, thermal oxidation of silicon, evaporation and patterning of Au, and filling the holes with Cu using Innovative Micro Technology (IMT) [28] “Super-fill” electroplating process (Figs. 4a and 4b). The thermal oxide is 2 μm thick and electrically isolates the TSVs from the bulk silicon. Since the copper reacts with the ionic liquid used while gold does not, prior to the Cu electroplating, a thin layer of Au was sputtered on the inner surfaces of the holes so that later the ionic liquid contacts the Au rather than Cu. After polishing down the over-plated Cu, a ~2 μm-thick Au were electroplated and patterned atop each Cu via to provide a bonding pad. The resistance of the TSV was measured less than 30 mΩ. After the TSV formation, the teeth pattern were defined by DRIE, which also etched an isolation trench and a breathing hole through the handle layer to the buried oxide layer (Fig. 4c).

Without a breathing hole, the air trapped in between two liquid rings, rotor and substrate will affect the device by factors such as temperature variation.

After flipping the SOI wafer, the device layer was thinned down to ~100 μm (Fig. 4d). Then, the top surface was made black silicon by DRIE in PlasmaTherm SLR770 ICP etcher (Unaxis Corporation) (Fig. 4e). During the ~10 min etching step, the gas flows of SF_6 and C_4F_8 was set to 30 sccm and 50 sccm, respectively, the ratio of etching and passivation time to 4s/5s, the coil power to 825 W, and the substrate temperature at ~20ºC. The polymer residues from the DRIE were cleaned in O_2 plasma (300 mTorr at 300 W) for 5 mins. A 2 wt% Teflon® AF 1600 solution was then spun-coated on the black silicon surface at 3000 rpm for 30 seconds and baked at 330ºC for 1 hour to make the surface superhydrophobic.

The last step of rotor/substrate fabrication was to define the wetting and non-wetting areas on the device layer and singulate the rotor (Fig. 4f). One key challenge here was to spin-coat a photoresist on the superhydrophobic (i.e., highly repellent) surface. To address the problem, the superhydrophobic surface was temporally wetted by immersing it in methanol and spun-coated with 8 μm-thick positive photoresist (AZ4620) before the methanol is completely evaporated. With the photoresist mask, two liquid grooves and one isolation trench were etched 100 μm deep by DRIE to the buried oxide. After removing the barrier oxide, the TSVs in the handle layer were uncovered at the bottom of the grooves. Finally, a ~200 nm-thick Au layer was evaporated, treated with O_2 plasma (300 mTorr at 300 W), and lifted off in a Piranha solution (4:1 H_2SO_4 and H_2O_2) leaving Au only inside the grooves (Fig. 4g). The Teflon on the black silicon surface after lift-off process was confirmed intact through visual inspection and contact angle measurement.

Figure 5 shows the fabrication result of the rotor. On the groove side of the rotor (i.e., the device-layer side of the SOI wafer), the non-wetting areas appear black, made of densely populated nanostructures having an apex of < 50 nm radius, height of 2–3 μm, and average pitch (i.e., period) of ~ 400 nm. Contact angle measurement showed that the non-wetting areas exhibited superhydrophobicity with a contact angle > 150º for ionic liquid EMIM

DCA. On the contrary, the surfaces inside the grooves were found superhydrophilic (contact angle ~ 0º).

B. Fabrication of Stators and Aligned Bonding with the Substrate

The set of six stators was made as one body from a 500 μm-thick highly doped silicon wafer (resistivity $\rho < 0.005$ Ω·cm) by DRIE with a 3 μm plasma-enhanced chemical vapor deposition (PECVD) oxide layer as the etching mask. After a thorough etching and cleaning, a 100 nm-thick Au layer was evaporated on the top side for an electrical contact. Then, the stator was glued with epoxy (Buehler EpoThin™) onto the substrate, which had already been bonded with a glass spacer while being aligned to the grooves (Fig. 1). The glass spacer was 100 – 200 μm thick, which is approximately the height of the liquid rings. Since the spacer is only to bring the stators to the rough vertical vicinity of the rotor, a simple glue bonding was good enough.

C. Assembly of Rotary Stage

Figure 6 shows the rotor-substrate assembly to complete the rotary stage for testing. Ionic liquid was manually dispensed into the wetting grooves both on rotor and substrate by using a micropipette. The liquid volume is critical for a successful assembly. Either too much or too little liquid resulted in a serious tilting or even collapsing of the assembled rotor. According to our experiments, liquid rings that result in a rotor-substrate gap of 100 – 200 μm provided a stable and non-tilting support. In order to achieve this target gap, the liquid volume for the inner ring and outer ring were controlled at 3 – 5 μL and 6 – 10 μL, respectively. After forming the two concentric liquid rings on the rotor and on the substrate, the rotor was flipped and lower to the substrate with a rough alignment to fit between the surrounding stators. When the rotor and substrate were close enough, the two sets of liquid rings merged into one set, pulling down and centering the rotor by surface tension.

IV. RESULTS AND DISCUSSION

A. Source of Static Resistance Against Rotation

One of the most important characteristics of micro rotational devices for electrostatic actuation is the startup

torque in order to overcome the static resistance against rotation. A perfect liquid ring would have no static resistance because there is no contact angle hysteresis, which means zero startup torque. In practice, however, a certain amount of torque is needed to initiate the rotation. In fact, a reduction of this startup torque was the breakthrough needed to make the side-drive electrostatic actuation even feasible in the first place. Note that the liquid-bearing devices with one large droplet at the center should also have a zero startup torque in theory, but the reality was far from the ideal condition [14], [15]. Therefore, a separate study [17] has been performed to understand the resistance of the liquid rings during the initial development. This section includes a summary of its experimental characterization performed with one ring (the outer ring) for simplicity. Note that one ring was used only in this section to study the source of static friction; two rings are used in all other sections. Using the minimum voltage measured that started the rotation, the startup torque was calculated using the FEM simulation. In this case, the minimum voltage that started a rotational movement was found to be ~50 V_{DC}, which corresponds to a startup torque of ~2.5 nN·m or ~100X smaller than the 0.3 μN·m on droplets [15]. Since the 3 cm rotor would experience ~3X larger torque than the 1 cm rotor [15] would for a given static friction, the static friction of the reported ring is considered ~300X smaller than that of the droplets.

In light of a focused investigation of capillary torque [18], the static resistance found in reality stemmed from the imperfect quality of the fabricated liquid grooves. Any deviation of the groove edges from a perfectly smooth arc would give rise to the resistance. Initially, we found that the resistance was mainly by the common defects in lithography, such as poor adhesion of photoresist on the superhydrophobic surface along the groove edges. During this early stage of development, the side-drive electrostatic force could not move the rotor at all even with an excessively high voltage (i.e. 800-1200 V) that made the rotor snap to the stators. As the process was improved and the liquid grooves were defined with no apparent defect, the rotational resistance was reduced dramatically and finally to the current status, allowing the side-drive electrostatic actuation at ~50 V_{DC}. The improvement included keeping the patterned photoresist fully intact during the DRIE of grooves (Fig. 4f). With regular photolithographic steps, the photoresist tended to peel off both during the DRIE process and the subsequent lift-off rather severely. We solved the problem by temporarily wetting the superhydrophobic surface with

methanol and using a thick and viscous photoresist AZ4620 for photolithography. Figure 7 shows the images of a typical liquid groove in this paper. Noting that the groove was etched by DRIE down from the surface of black silicon (full of ~400 nm-pitch and 2-3 μm-tall nanostructures) with a photoresist patterned on them, it was not surprising to find the top edge defined fuzzy within a ~2 μm zone, as shown in the magnified image (Fig. 7a). As a result, the liquid-air interface, which is defined by the edge, was not perfectly smooth, either (Fig. 7b), as schematically explained by the exaggeratedly wavy meniscus in Fig. 7c. The wavy meniscus near the solid-liquid interface poses an energy barrier against rotation. When the meniscus height, i.e., the rotor-substrate gap, decreased to be comparable to the magnitude of edge roughness, the resistance became more prominent [17], [29]. Therefore, the edge roughness of the groove should be taken into consideration when one designs the liquid ring bearing.

B. Continuous Electrostatic Actuation

The assembled rotary stage has been run successfully with stepwise rotation by programming the driving voltage phase in an appropriate sequence, which includes both clockwise and counterclockwise rotations. The test was performed with the device fully exposed to air on a folding table (i.e., not a clean and sturdy laboratory table) in a carpeted room for more than 10 hours continuously. The rotation was open-controlled (i.e., no feed-back control) with a constant excitation frequency of ~0.6 Hz, and the speed was kept at a rate of ~5º/s at all times. No collapsing or apparent tilting of the rotor was observed.

C. Power Transmission by Ionic Liquid Ring Bearings

In order to verify the electrical power transmission onto a rotating rotor, a light-emitting diode (LED, Nichia NSPG520AS, InGaN green LED) was mounted on top of the rotor and electrically connected to the Au bonding pads as shown in Fig. 8. The rotor on two ionic liquid rings was rotated electrostatically by applying a three-phase voltage of 100 V_{DC} between the stators and rotor. Note that 100 V_{DC} would generate a torque 4 times lager than what 50 V_{DC} would, while two rings would resist against rotation roughly twice what a single ring would. We speculate that the additional resistance was caused by the less-than-perfect volume control of the two rings. At the

same time, the LED was powered separately by another power supply. For the LED operation, a chain of 4 V_{DC} pulses was applied to the substrate vias, across each of the two liquid rings, through corresponding TSVs, and to the LED on the rotor with ~0.1 mA of current. Figure 8b shows the sequential photos during rotation. The power transmission was within the electrochemical window of the ionic liquid to avoid electrolysis, as discussed in the Principles and Design section. Blinking of the LED was successfully demonstrated while the rotor was electrostatically rotated at ~5º/s, confirming all the main features of the proposed rotary stage. Because the current device, which lacks a position sensing and feedback-controlled actuation, is limited to a low angular speed by the electrostatic actuation, the power transmission at high-speed rotation was further tested at ~300 rpm by blowing air to the rotor through a capillary. Figure 9 shows the photo during high speed rotation. The LED operation was equally successful with the same 4 V_{DC} input as above, resulting in the same current of ~0.1 mA, indicating that high-speed rotation does not affect the power transmission of ionic liquid ring bearings.

D. Further Discussion

The weight of rotor, LED, and bonding wires was ~0.7 g, demonstrating a payload capability of the liquid-ring bearings. In order to verify the stability of liquid-ring bearing, a volume monitoring experiment was carried out by placing a droplet of ionic liquid EMIM DCA in the atmosphere at room temperature for over 30 hours. A CCD camera connected to a PC was used to monitor the droplet through the experiment. Estimated by counting the pixels of each droplet images, the droplet was found to change its volume less than 10% over 30 hours. Besides, an assembled rotary stage device functioned normally after 3 weeks of storage on the shelf without any protective packaging.

Compared with most other bearings, a drawback of liquid-ring bearing would be the possibility of rotor tilting, which may be caused by inappropriate liquid volume, eccentrically placed payload on the rotor, external disturbances, etc. In order to prevent the tilting, we controlled the dispensing of ionic liquid into the grooves and placed the payload at the center of the rotor. Detailed numerical studies about tilting are included in [17]

In this initial development, we have not attempted to achieve a fast rotation, which would require a bottom-driven (vs. the current side-driven) actuation to increase the electrostatic force and a real-time position sensing to implement a feedback-controlled actuation

Although we do not report any application, the rotary stage developed in this paper has a unique potential as a rotating platform for other miniaturized devices. For example, it may provide a portable calibration platform for micro inertial devices. In this case, both input and output signals to and from the devices on the rotor are transmitted through the substrate, ionic liquid, and TSV.

V. CONCLUSION

We have successfully demonstrated rings of a conductive liquid as both mechanical bearings and electrical connections. Fabrication of defect-free liquid rings has been the key to achieve a very small static friction – small enough to allow rotation by side-driven electrostatic actuation. The stability and reliability of liquid-ring bearing have also been verified through a long-term testing. A direct electrical power transmission to an infinitely rotating device has been demonstrated for the first time, which opens a new application window for miniature rotating devices.

ACKNOWLEDGEMENTS

The authors thank Prof. C.-K. Ken Yang and Mr. Jong Jin Kim for their help on the electrostatic actuation test and Prof. Sangwoo Lim for his advice on choosing the ionic liquid. This work is supported by the Defense Advanced Research Projects Agency (DARPA) under grant W31P4Q-10-1-0008.

REFERENCES

[1] L.-S. Fan, Y.-C. Tai, and R.S. Muller, "IC-Processed Electrostatic Micromotors," *Sensors and Actuators*, vol. 20, pp.41-47, 1989.

[2] M. Mehregany, S. F.Bart, L. S. Tavrow, J. H. Lang, "Principles in Design and Microfabrication of Variable-Capacitance Side-Drive Motors," *J. Vac. Sci. Technol. A*, vol. 8, pp. 3614-3624, 1990.

[3] N. Ghalichechian, A. Modafe, M. L. Beyaz, and R. Ghodssi, "Design, Fabrication, and Characterization of a Rotary Micromotor Supported on Microball Bearings," *J. Microelectromech. Syst.*, vol. 17, pp. 632-642, 2008.

[4] M. McCarthy, C.M. Waits, M. I. Beyaz, and R. Ghodssi, "A Rotary Microactuator Supported on Encapsulated Microball Bearings Using An Electro-Pneumatic Thrust Balance," *J. Micromech. Microeng.*, vol. 19, pp. 1-7, 2009.

[5] P. Muralt, "Ultrasonic Micromotors Based on PZT Thin Films," *J. Electroceramics*, vol. 3, pp. 143-150, 1999.

[6] C. H. Ahn, Y. J. Kim, and M. G. Allen, "A Planar Variable Reluctance Magnetic Micromotor with Fully Integrated Stator and Coils," *J. Microelectromech. Syst.*, vol. 2, pp. 165-173, 1993.

[7] M. Mehregany, S.D. Senturia, and J.H. Lang, "Measurement of Wear in Polysilicon Micromotors," *IEEE Transactions on Electron Devices*, 39, pp. 1136-1143, 1992.

[8] L.G. Frechette, S.F. Nagle, R. Ghodssi, S.D. Umans, M.A. Schmidt, J.H. Lang, "An Electrostatic Induction Micromotor Supported on Gas-lubricated Bearings," *Proc. IEEE Int. Conf. MEMS*, Interlaken, Switzerland, pp. 290–293, Jan. 2001.

[9] C. W. Wong, X. Zhang, S. A. Jacobson, and A. H. Epstein, "A Self-Acting Gas Thrust Bearing for High-Speed Microrotors," *J. Microelectromech. Syst.*, vol. 13, pp. 158–164, 2004.

[10] L. G. Fréchette, S. A. Jacobson, K. S. Breuer, F. F. Ehrich, R. Ghodssi, R. Khanna, C. W. Wong, X. Zhang, M. A. Schmidt, and A. H. Epstein, "High-Speed Microfabricated Silicon Turbomachinery and Fluid Film Bearings," *J. Microelectromech. Syst.*, vol. 14, pp. 141–152, Feb. 2005.

[11] J. U. Jeon, S. J. Woo, and T. Higuchi, "Variable-Capacitance Motors with Electrostatic Suspension," *Sensors and Actuators A*, vol. 75, pp. 289-297, 1999.

[12] C. Shearwood, K. Y. Ho, C. B. Williams, and H. Gong, "Development of a Levitated Micromotor for Application as a Gyroscope," *Sensors and Actuators A*, vol. 83, pp. 85-92, 2000.

[13] A. Takei, K. Matsumoto, and I. Shomoyama, "Capillary Motor Driven by Electrowetting,",*Lab Chip.*, vol. 10, pp. 1781-1786, 2010.

[14] M. L. Chan, B. Yoxall, H. Park, Z. Kang, I. Izyumin, J. Chou, M. M. Megens, M. C. Wu, B. E. Boser, and D. A. Horsley, "Design and Characterization of MEMS Micromotor Supported on Low Friction Liquid Bearing," *Sensors and Actuators A*, vol. 177, pp. 1– 9, 2012.

[15] B.E. Yoxall, M. Chan, R. S. Harake, T. Pan, and D.A. Horsley, "Rotary Liquid Droplet Microbearing," *J. Microelectromech. Syst.*, vol. 21, pp.721-729, 2012.

[16] G. Sun, T. Liu, P. Sen, W. Shen, C. Gudeman, and C.-J. Kim, "Electrostatically Driven Rotor on Conductive Liquid Ring Bearings," Technical Digest, Solid-State Sensor, *Actuator and Microsystems Workshop*, Hilton Head Island, SC, pp. 78-81, June 2012.

[17] Y. Zhan, "Study of Characteristics of Liquid-Based Bridge Structure as Mechanical Elements," *M.S. Dissertation & Theses @University of California, Los Angeles*, 1511895, 2012.

[18] T. Liu, P. Sen, and C.-J. Kim, "Characterization of Nontoxic Liquid-Metal Alloy Galinstan for Applications in Microdevices," *J. Microelectromech. Syst.*, vol. 21, pp. 443-450, 2012.

[19] M. H. Ghatee, M. Zare, A. R. Zolghadr, F. Moosavi, "Temperature Dependence of Viscosity and Relation with the Surface Tension of Ionic Liquids," *Fluid Phase Equilibria*, vol. 291, pp. 188–194, 2010.

[20] R. Osada, T. Hoshino, K. Okada, Y. Ohmasa, and M. Yao, "Surface Tension of Room Temperature Ionic Liquids Measured by Dynamic Light Scattering," *J Chem Phys.*, vol. 130, 184705, 2009.

[21] D. R. MacFarlane, J. Golding, S. Forsyth, M. Forsyth and G. B. Deacon, "Low Viscosity Ionic Liquids Based on Organic Salts of the Dicyanamideanion," *Chem. Commun.*, pp. 1430–1431, 2001.

[22] S. I. Fletcher, F. B. Sillars, N. E. Hudson, and P. J. Hall, "Physical Properties of Selected Ionic Liquids for Use as Electrolytes and Other Industrial Applications," *J. Chem. Eng. Data*, vol. 55, pp. 778–782, 2010.

[23] Y. Liu, R. Zhao, M. Ghaffari, J. Lin, S. Liu, H. Cebeci, R. G. de Villoria, R. Montazami, D. Wang, B. L. Wardle, J. R. Heflin, Q.M. Zhang, "Equivalent Circuit Modeling of Ionomer and Ionic Polymer Conductive Network Composite Actuators Containing Ionic Liquids," *Sensors and Actuators A* , vol. 181, pp. 70– 76, 2012.

[24] B. Gassend, L. F. Velásquez-García, A. I. Akinwande, and M.l Martínez-Sánchez, "A Microfabricated Planar Electrospray Array Ionic Liquid Ion Source With Integrated Extractor," *J. Microelectromech. Syst*, vol. 18, pp. 679-694, 2009.

[25] Ionic Liquids Database- (ILThermo), *NIST Standard Reference Database* #147, © 2006, US Secretary of Commerce.

[26] W. C. Tang, T.-C. H. Nguyen, and R. T. Howe, "Laterally Driven Polysilicon Resonant Microstructures," *Sensors and Actuators*, vol. 20, pp. 25-32, 1989.

[27] W. C. Tang, T.-C. H. Nguyen, M. W. Judy, and R. T. Howe, "Electrostatic-comb Drive of Lateral Polysilicon Resonators," *Sensors and Actuators*, A21-A23, pp. 328-331, 1990.

[28] http://www.imtmems.com/index.php/technology.html#through_silicon

[29] A. Takei, K. Matsumoto, and I. Shimoyama, "Capillary Torque Caused by a Liquid Droplet Sandwiched between Two Plates," *Langmuir*, vol. 26, pp. 2497-2504, 2009.

Guangyi Sun received the B.S. degree in computer science and technology from Tianjin University, Tianjin, China, in 2004, and the M.S. and Ph.D. degrees in control theory and control engineering from Nankai University, Tianjin, China, in 2007 and 2010, respectively.

From 2008 to 2010, he was a joint Ph.D. student at the University of California, Los Angeles (UCLA). Since 2010, he has been a postdoctoral researcher at UCLA. His research interests are in MEMS and nanotechnology.

Tingyi "Leo" Liu received the B.Eng. degree in electrical engineering (with honors) from Zhejiang University, Hangzhou China, in 2009, and the M.S. degree in mechanical engineering from the University of California, Los Angeles (UCLA), in 2011. He is currently working toward the Ph.D. degree in mechanical engineering at the University of California, Los Angeles (UCLA). Working in the Micro and Nano Manufacturing Laboratory, UCLA, his research interests include engineering designs utilizing capillarity, liquid-metal based micro devices, and micro gyroscope systems.

Prosenjit Sen was born in Calcutta, India, in 1978. He received the Ph.D. degree in mechanical engineering from the University of California, Los Angeles (UCLA), in 2007, and the B.Tech. degree in manufacturing science and engineering from the Indian Institute of Technology, Kharagpur, India, in 2000.

At the Micro and Nano Manufacturing Laboratory, UCLA, his research interests included microfluidic systems, droplet dynamics, liquid-metal-based RF microelectromechanical systems, and reliability of electrowetting-on-dielectric devices. From 2010-2013 he worked at Innovative Micro Technology, Santa Barbara, CA as a process engineer and program manager. Currently he is an Assistant Professor in Centre for Nano Science and Engineering at Indian Institute of Science.

Dr. Sen is a recipient of the Institute Silver Medal from the Indian Institute of Technology, Kharagpur.

Wenjiang Shen received the B.S. and M.S. degrees from materials science and engineering from Tsinghua University, China. He got his Ph.D. degree in mechanical engineering from UCLA in 2004.

He worked as a process engineer and program manager in Innovative Micro Technology (IMT) from 2005 to 2011. He is currently a professor in Suzhou Institute of Nano-tech and Nano-Bionics, Chinese Academy of Sciences. His research areas include micro-system integration and energy conversion in micro/nano scale.

Chris Gudeman received his PhD in Chemistry from the University of Wisconsin. His thesis work won him the ACS Nobel Laureate Signature Award and the Council of Graduate Schools in the USA Distinguished Dissertation Award. He is currently CTO at Innovative Micro Technology in Santa Barbara, CA.

Chang-Jin "CJ" Kim received the B.S. degree from Seoul National University, Seoul, Korea, the M.S. degree from Iowa State University, Ames, and the Ph.D. degree from the University of California, Berkeley, in 1991, all in mechanical engineering.

Since joining the faculty at the University of California, Los Angeles (UCLA), in 1993, he has developed several courses in microelectromechanical system (MEMS) and established a MEMS Ph.D. major field in the Mechanical and Aerospace Engineering Department in 1997. Directing the Micro and Nano Manufacturing Laboratory, he is also a founding member of the California NanoSystems Institute (CNSI) at UCLA. His research interests are in MEMS and nanotechnology, including design and fabrication of micro/nano structures, actuators, and systems, with a focus on the use of surface tension.

Prof. Kim has served on numerous technical committees and panels, including Transducers, the IEEE International Conference on MEMS, and the National Academies Panel on Benchmarking the Research Competitiveness of the U.S. in Mechanical Engineering. He is currently serving on the Steering Committee and the Editorial Board for the Journal of Microelectromechanical Systems, on the Editorial Advisory Board for the IEEJ Transactions on Electrical and Electronic Engineering, and as Co-Chair of the 27th IEEE International Conference on Micro Electro Mechanical System. A fellow of ASME, he was the recipient of the Graduate Research Excellence Award from Iowa State University, the 1995 TRW Outstanding Young Teacher Award, the 1997 NSF CAREER Award, the 2002 ALA Achievement Award, and the 2008 Samueli Outstanding Teaching Award.

Table I The proposed liquid-ring bearing compared with the bearings in other reported micro rotating devices

Bearing		**Solid**		**Gas**	**Liquid**	
		Slide[1,2]	Roll[3,4]	Levitation[8-10]	Droplet[13-15]	Ring
Friction	Static	Sliding	Rolling	No static friction	Contact angle hysteresis	None static friction
	Dynamic			Gas shear	Liquid shear	Liquid shear
Issues		Large friction; Durability	Sliding remains	Complex control; Stability limit	Evaporation; Rotor tilting; Large drag	Static friction in reality
Material used		Silicon; Silicon nitride	Stainless steel; silicon carbide	Gas	Water; Ethylene glycol	Ionic liquid
Method of rotation		Electrostatic		Electrostatic	Magnetic; Electrowetting	Electrostatic; Pneumatic
Electric transmission		Electrical power can not be directly delivered on to the rotor				Possible

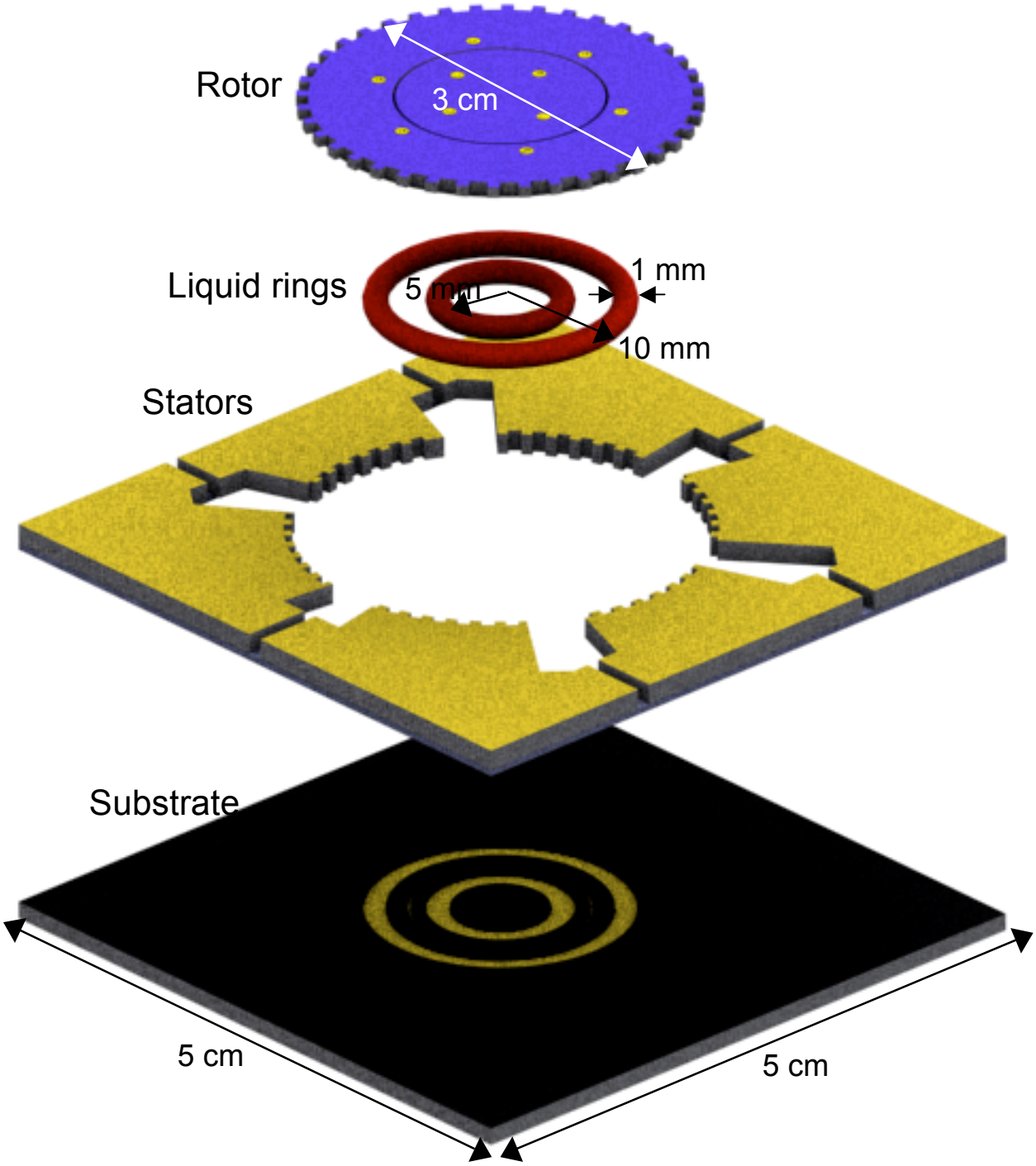

Fig. 1 Exploded view of the side-driven rotary stage on conductive liquid rings.

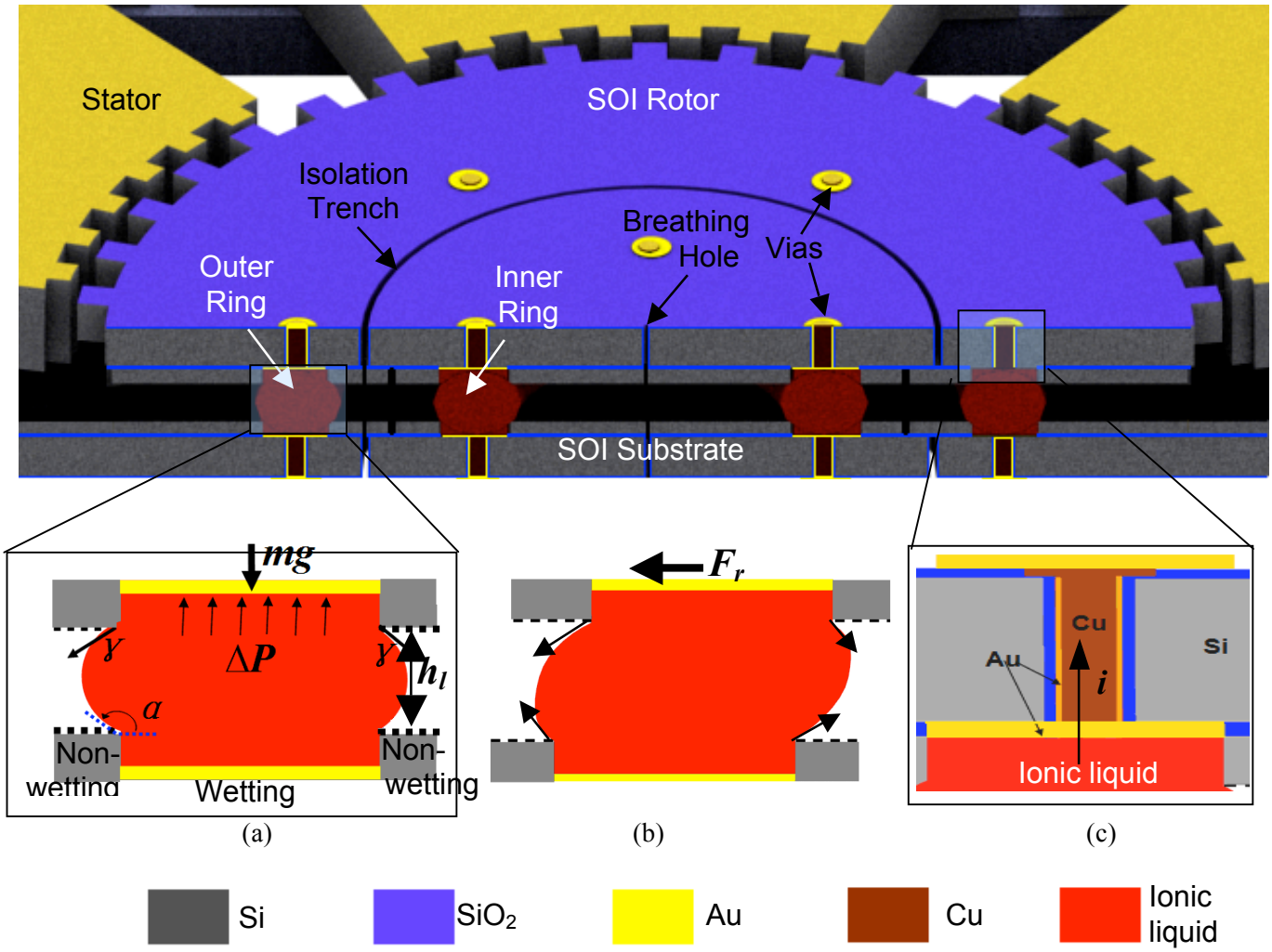

Fig. 2 Assembled rotary stage with a cut-out view and cross-sectional details. (a) Vertical stability provided by Laplace pressure. (b) Horizontal stability provided by surface tension. (c) Electric transmission through liquid ring and via.

Table II Geometric specifications of the liquid-ring bearing electrostatic rotary stage

Specification	**Value**
Diameter of rotor	30 mm
Thickness of rotor	350 μm
Stator thickness	500 μm
Number of teeth (rotor/stator)	56/42
Rotor-stator gap (*g*)	100 μm
Rotor-substrate gap (*h*)	100-200 μm
Depth of liquid groove	100 μm
Number of liquid rings	2
Diameter of inner/outer liquid ring	5/10 mm
Width of liquid rings	1 mm

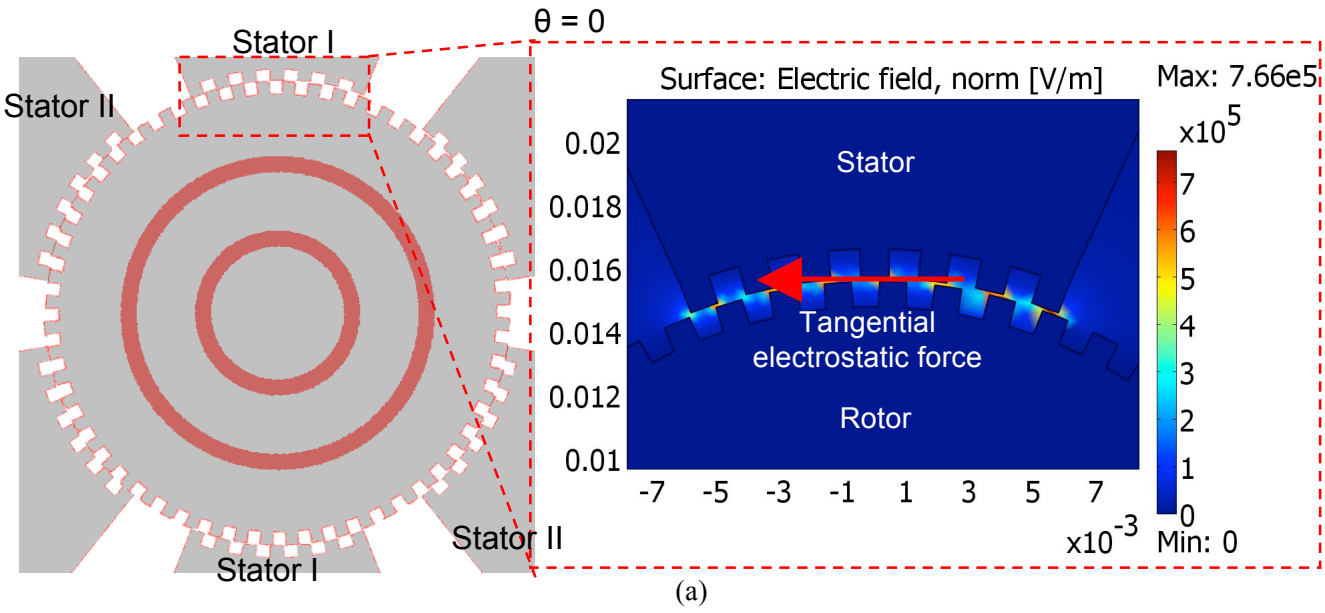

(a)

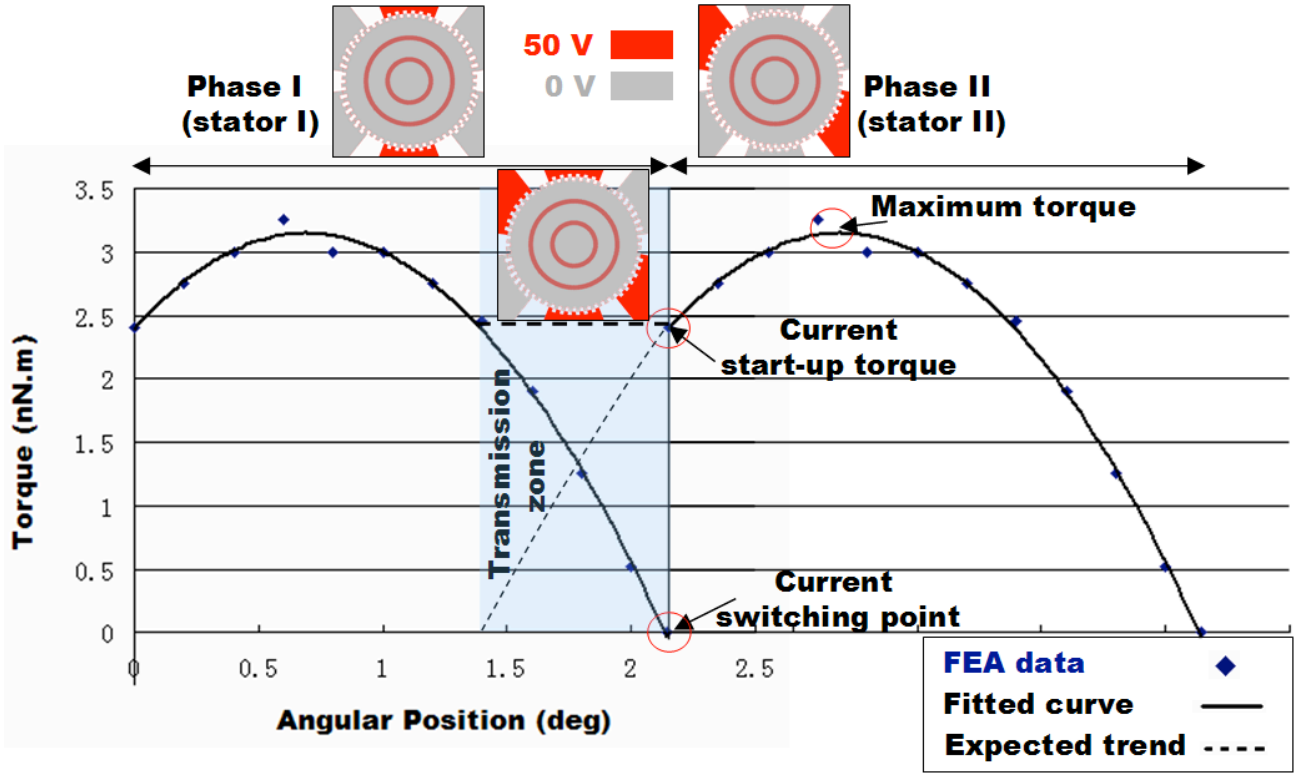

(b)

Fig. 3 FEA simulation of electrostatic actuation. (a) 2D model of the rotary stage and the electrostatic field between the rotor and an active stator. (b) The torque on the rotor by the stators versus the angular position of the rotor.

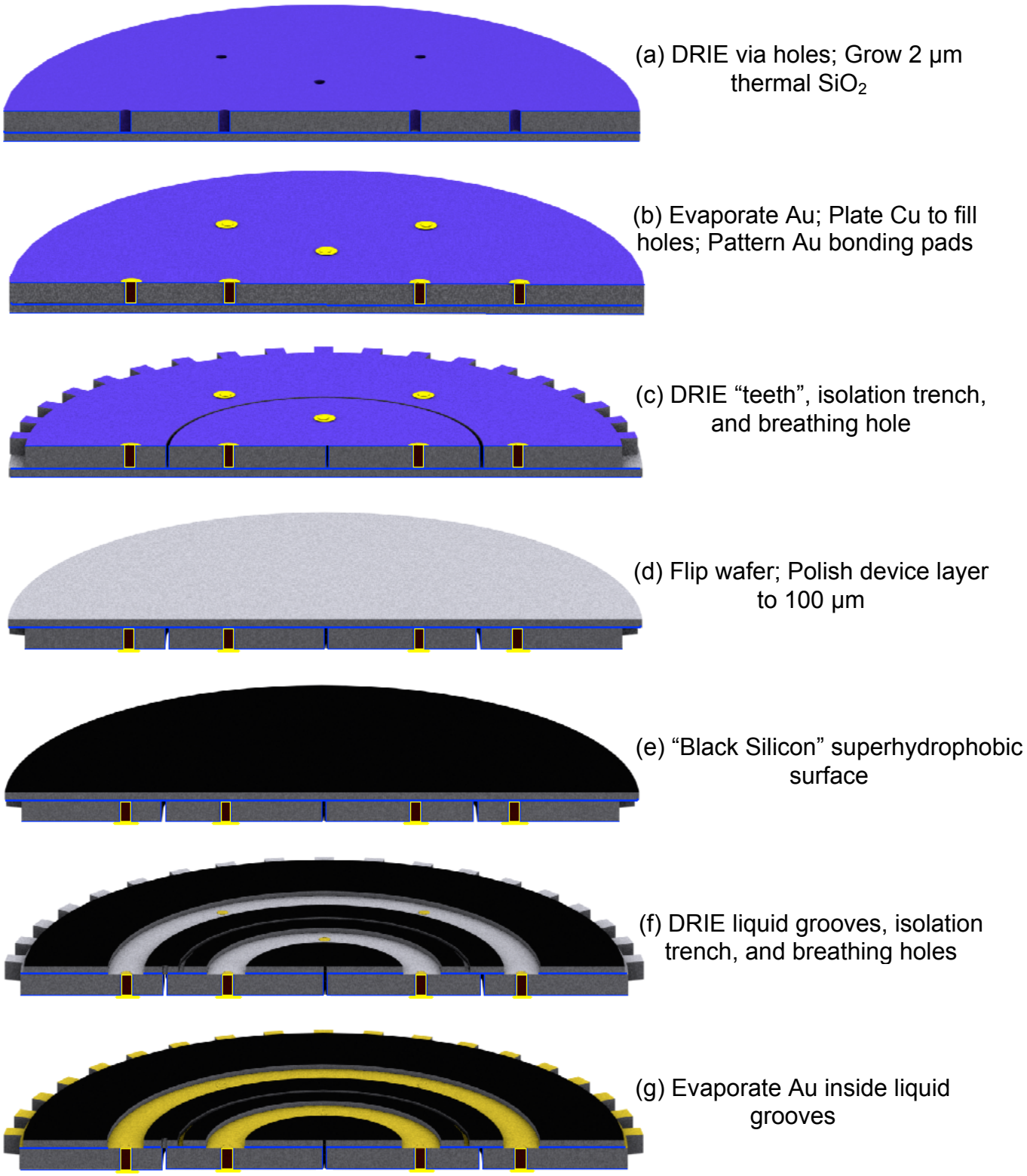

Fig. 4 Process flow to fabricate the rotor, starting with an SOI wafer.

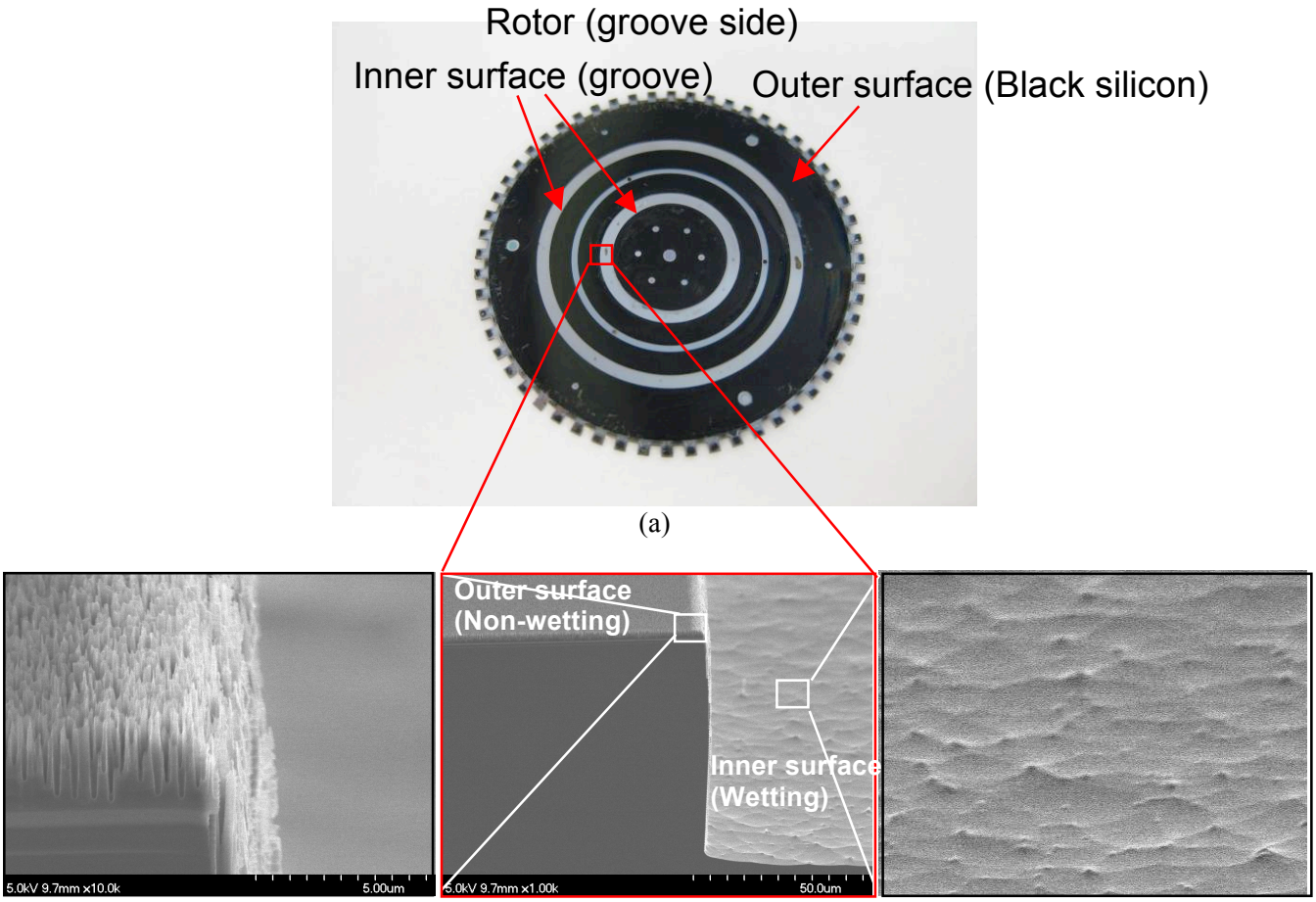

Fig. 5 Fabrication results. (a) Optical picture of the rotor (flipped to show the bottom surface) (b) SEM pictures of a rotor (broken to reveal the cross section), showing the groove area around the edge (center), the top outer non-wetting surface (left), and the bottom inner wetting surface (right).

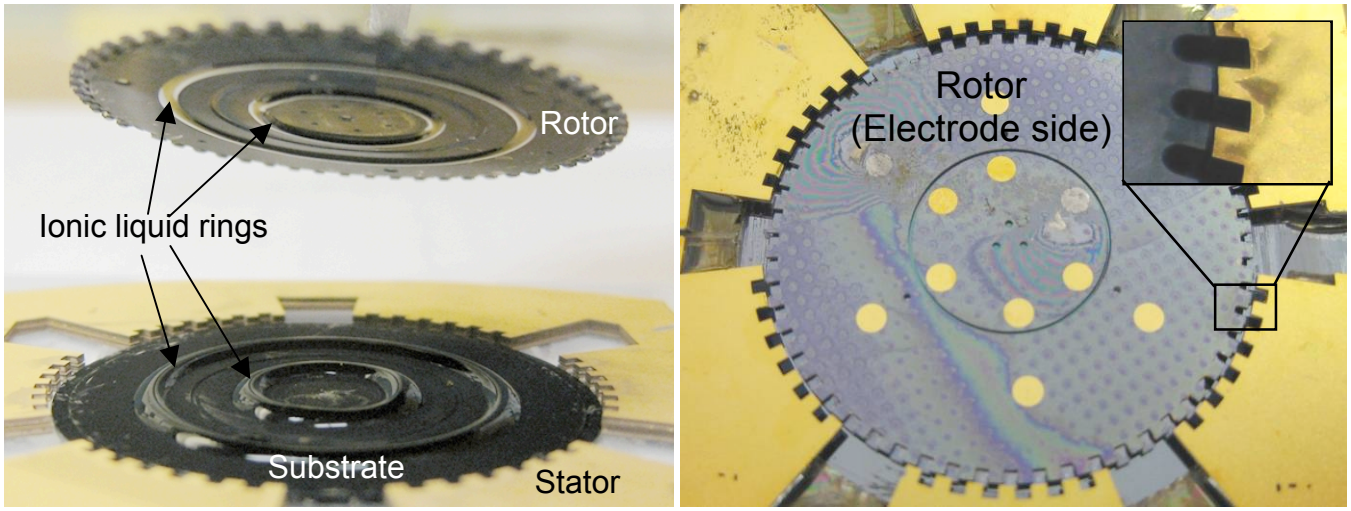

(a) (b)

Fig. 6 Assembly of rotary stage. (a) The rotor is being assembled with the substrate by two ionic liquid rings. (b) Assembled device maintains a specified rotor-substrate gap determined by the liquid volume and keeps the rotor centered by the surface tension.

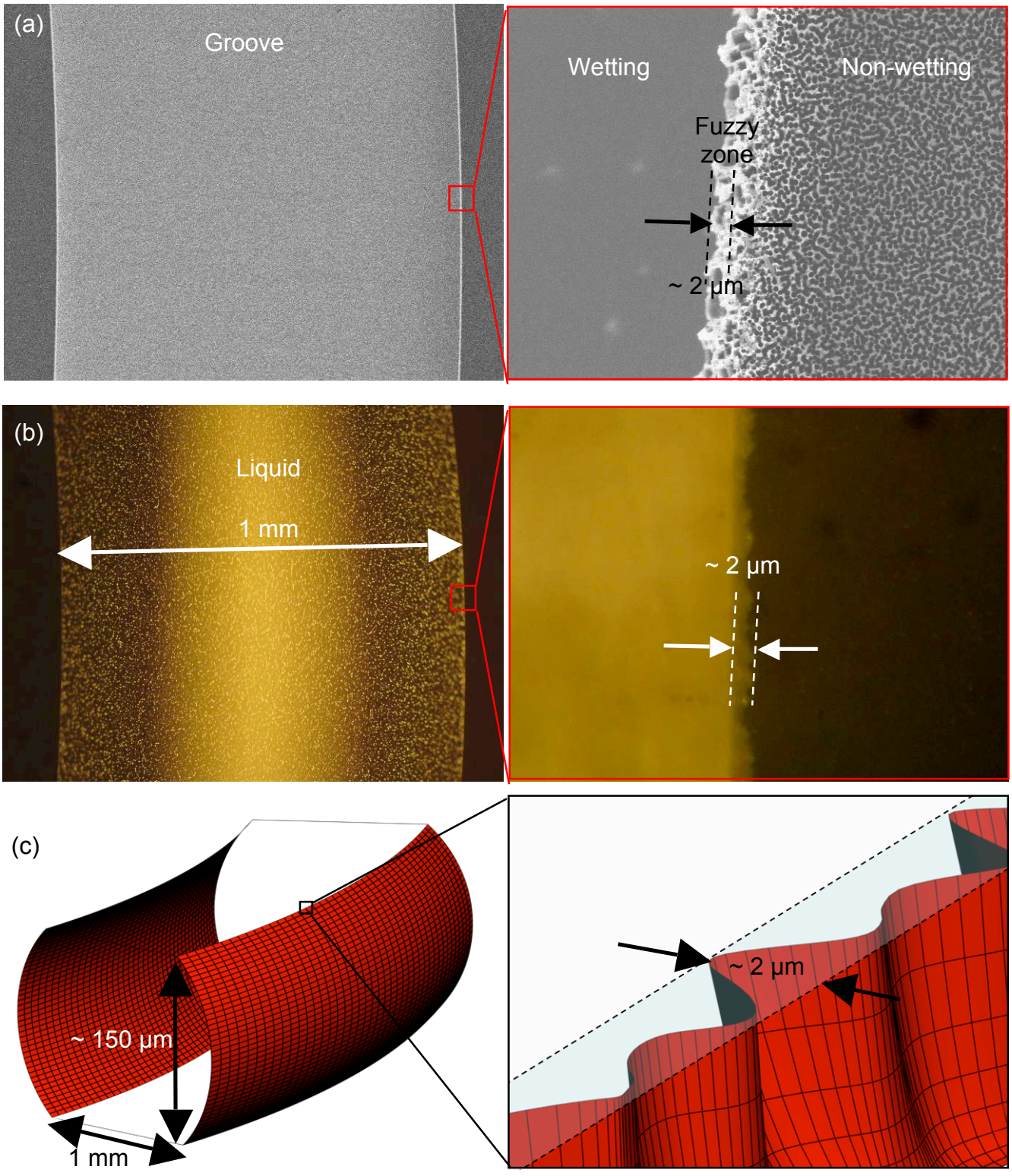

Fig. 7 Study of contact line reveals the origin of the resistance against rotation. (a) SEM images of the groove and magnified for the top edge. (b) Optical micrographs of liquid inside groove and magnified for the contact line. (c) Schematic of the contact line on the fuzzy edge. Drawn not to scale.

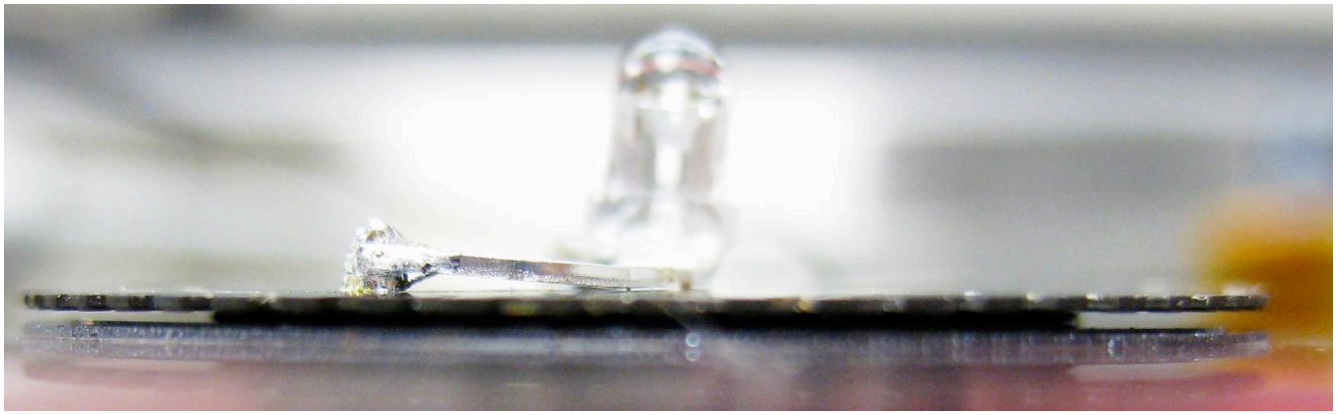

(a)

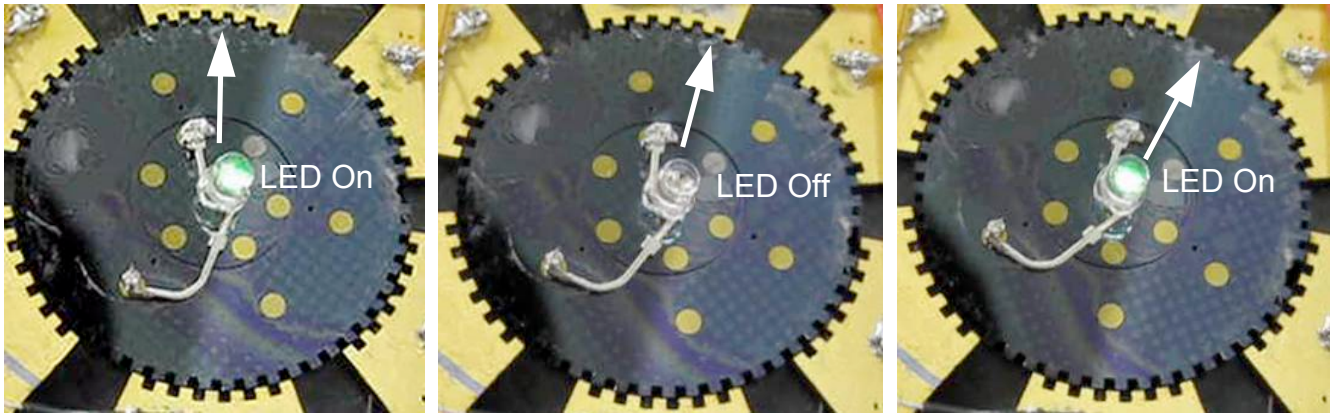

(b)

Fig. 8 Demonstration of power transmission by ionic liquid rings bearing. (a) Side-view of an assembled rotor without out stators showing the liquid rings. (b) Electrostatic actuation with a blinking LED on the rotor. The white arrow indicates the rotated angle.

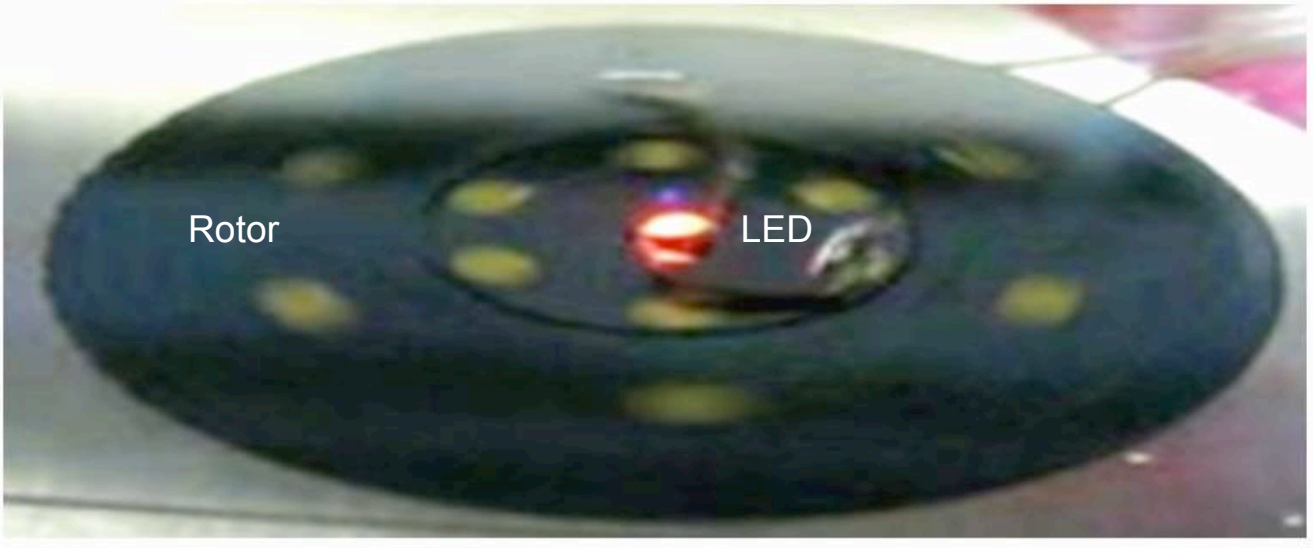

Fig. 9 A red LED blinking at the center of a rotor (no stator in this device) that is being rotated by blowing air.